Single domain antibody-antigen adducts that target Class II MHC induce antigen-specific tolerance

Novalia Pishesha (novalia.pishesha.168@gmail.com)
Boston Children's Hospital

Thibault Harmand
Boston Children's Hospital

Liyan Smeding
Boston Children's Hospital

Weiyi Ma
Boston Children's Hospital

Leif Ludwig
Broad Institute of MIT and Harvard https://orcid.org/0000-0002-2916-2164

Robine Janssen
Boston Children's Hospital

Ashraful Islam
Boston Children's Hospital

Yushu Xie
Boston Children's Hospital

Tao Fang
Boston Children's Hospital

Nicholas McCaul
Boston Children's Hospital https://orcid.org/0000-0002-7888-7815

William Pinney
Boston Children's Hospital

Harun Sugito
Boston Children's Hospital

Hidde Ploegh
Boston Children's Hospital-Harvard Medical School

Article

Keywords: autoimmunity, autoimmune diseases, Class II MHC, antibodies, antigen

Posted Date: February 11th, 2021

DOI: https://doi.org/10.21203/rs.3.rs-192181/v1

Version of Record: A version of this preprint was published at Nature Biomedical Engineering on June 14th, 2021. See the published version at https://doi.org/10.1038/s41551-021-00738-5.

Abstract

The association of autoimmune diseases with particular allelic variants of Class II MHC (MHCII) products implicates presentation of the offending self-antigen(s) to T cells. Antigen presenting cells are tolerogenic when they encounter antigen under non-inflammatory conditions. Manipulation of antigen presentation would therefore be a possible intervention to induce antigen-specific tolerance. We show that, under non-inflammatory conditions, systemic administration of a single dose of a nanobody that recognizes MHCII (VHH MHCII) conjugated to the relevant self-antigen affords long-lasting protection against induction of experimental autoimmune encephalitis (EAE), type 1 diabetes (T1D), and rheumatoid arthritis (RA). Co-administration of the VHH MHCII-antigen adduct together with dexamethasone, conjugated to VHH MHCII via a cleavable linker, not only halted progression of established EAE in symptomatic mice but even reverted the severity of EAE, establishing this approach as a potential means of treating autoimmune conditions.

Introduction

Approximately 10% of the human population suffer from an autoimmune condition, with symptoms that range from mild to life-threatening [1]. Current treatments for autoimmune diseases include general immunosuppression, which blunts responses across the entire spectrum of antigens. Various preclinical models of autoimmunity involve administration of a defined antigen under the appropriate stimulatory conditions to elicit pathology [2]. Engagement of antigen presenting cells (APCs) under inflammatory conditions, e.g., in the presence of adjuvants, elicits a strong response against foreign antigens [3, 4]. In contrast, APCs that acquire antigen under non-inflammatory conditions fail to upregulate costimulatory signals and induce tolerance [5, 6]. To target APCs under tolerogenic conditions, we developed and characterized alpaca-derived single domain antibody fragments (nanobodies/VHHs) that recognize Class II MHC molecules (VHH_{MHCII}) [7, 8]. These nanobodies lack effector functions and target all MHCII-positive cells, which include APCs. Their small size ensures efficient tissue penetration and rapid clearance from the circulation of those nanobodies that fail to find their target. This makes nanobodies ideal vehicles for targeted delivery of payloads of interest, such as antigenic peptides or small molecule drugs [9, 10]. We have further established an engineering strategy for nanobodies that enables their site-specific modification at their C-terminus with the aforementioned payloads [11].

The distribution of a diverse set of APCs over different anatomical sites and their cellular dynamics complicate the identification of the relevant tolerogenic APC *in vivo*. The possible transfer of materials between various sets of APCs is an additional confounding factor. In fact, several distinct types of APCs or their products could all contribute and act in synergy to induce tolerance [12]. Here, we demonstrate the efficacy of using VHHs that target the MHCII-positive cell population as tolerogens. This approach was effective in prevention and treatment of experimental autoimmune encephalitis (EAE), in an accelerated model of type I diabetes in the mouse and in a T cell-mediated arthritis model. To extend this approach to disease interception, we delivered dexamethasone, an immunosuppressive small molecule, to MHCII-positive cells via VHH_{MHCII} conjugated to dexamethasone through a cleavable linker. We find that

VHH_{MHCII}-peptide adducts in combination with VHH_{MHCII}-dexamethasone are an effective treatment of animals symptomatic for EAE: it halts disease progression in animals with overt signs of disease.

Results

A single dose of VHH_{MHCII}-MOG_{35-55} provides durable protection against induction of experimental autoimmune encephalomyelitis (EAE). We engineered an alpaca-derived single domain antibody that recognizes a wide range of mouse Class II MHC molecules (MHCII), including I-A^b and I-A^d (VHH_{MHCII}), with a sortase recognition motif - LPETGG - to allow its site-specific ligation (Fig. 1a) to antigenic peptides and small molecules modified with (a) suitably exposed glycine residue(s). Purified VHH adducts were characterized by LC-MS (Fig. 1b and Supplementary Fig. 1) to verify identity.

Immunization of C57BL/6 mice with MOG_{35-55} in the presence of complete Freund's adjuvant (CFA) and pertussis toxin (PTX) elicits experimental autoimmune encephalitis (EAE), a multiple sclerosis-like condition [13]. We hypothesized that prior administration of MOG_{35-55}, delivered to MHCII+ APCs under non-inflammatory conditions, might interfere with the induction of EAE. We administered 3 doses of 20mg of the VHH_{MHCII}-MOG_{35-55} adduct intravenously, 7 days prior to induction of disease. This treatment suppressed induction of EAE. Mice that received the identical amount of VHH_{MHCII} conjugated to an irrelevant peptide (VHH_{MHCII}-$OVA_{323-339}$) or MOG_{35-55} peptide linked to a VHH of irrelevant specificity (VHH_{GFP}) invariably developed EAE (Fig. 1c, Supplementary Fig. 2). Even a single injection of 20mg VHH_{MHCII}-MOG_{35-55} still achieved full protection (Fig. 1d and e, Supplementary Fig. 2); a dose used in all subsequent experiments. Flow cytometry of CD4+ lymphocyte infiltrates recovered from the spinal cord of diseased mice at day 15–18 after immunization and of protected mice at day 30 after administration of the MOG_{35-55}/CFA/PTX cocktail was consistent with the observed disease scores: diseased mice showed a pronounced influx of IL-17 and IFNg-producing CD4+ T cells as well as some Foxp3+ CD4+ regulatory T cells (Fig. 1f, Supplementary Fig. 2). H&E and Luxol Fast Blue staining of spinal cord sections from mice that received VHH_{MHCII}-MOG_{35-55} prior to attempts to induce EAE showed preservation of myelination and less immune cell infiltration (Figs. 1g and 1h).

To explore the durability of protection afforded by VHH_{MHCII}-MOG_{35-55}, we injected 20mg of VHH_{MHCII}-MOG_{35-55} one or two months prior to administration of the MOG_{35-55}/CFA/PTX cocktail. Even then we observed delayed onset, if not complete suppression of EAE (Fig. 1i, Supplementary Fig. 3). In spite of the short circulatory half-life of free VHH_{MHCII}-MOG_{35-55}, estimated to be < 0.5 hour, VHH_{MHCII}-MOG_{35-55} confers prolonged protection. Five weeks after the VHH_{MHCII}-MOG_{35-55} injection, which established protection to a first exposure to MOG_{35-55}/CFA/PTX, we re-challenged mice with a second administration of MOG_{35-55}/incomplete Freund's adjuvant (IFA) in the presence of PTX. Despite this second challenge, mice, once protected, showed no signs of developing EAE (Fig. 1j, Supplementary Fig. 4). Tolerance evoked by a single dose of VHH_{MHCII}-MOG_{35-55}, even weeks after its administration, thus provides lasting protection to even a second challenge.

Splenic CD11c+ DCs are the APCs associated with induction of antigen-specific tolerance. To explore possible mechanisms of VHH_{MHCII}-mediated induction of tolerance, we generated VHH_{MHCII}-Alexa 647 (Supplementary Fig. 5) to follow the biodistribution of VHH_{MHCII}-Alexa647, injected i.v. into MHCII-GFP mice. These mice carry a targeted gene replacement that encodes an I-A^b-GFP fusion. It replaces the endogenous I-A^b locus and ensures that all Class II MHC+ cells express GFP [14]. At 1.5 hrs after injection, VHH_{MHCII}-Alexa647 is captured by a splenic and circulatory MHCII-GFP+ cell population (Fig. 2a). The fluorescent VHH_{MHCII} adducts were captured by B cells and DC subsets, including splenic CD8a+ DCs, CD4- conventional DCs (cDCs), as well as CD4+ cDCs, but not plasmacytoid DCs (Supplementary Fig. 6).

Intravenous, but not subcutaneous or intraperitoneal injection of VHH_{MHCII}-MOG_{35-55} protected against induction of EAE (Supplementary Fig. 7). This hinted at a role of the spleen or the bloodstream as a site where tolerance induction is initiated. One week after injection of 20mg of VHH_{MHCII}-MOG_{35-55} i.v. (Fig. 2b, Supplementary Fig. 8), we harvested their splenocytes and whole blood as a source of donor cells. Mice then received 20 millions unfractionated splenocytes or peripheral blood mononuclear cells (PBMCs) from the VHH_{MHCII}-MOG_{35-55} treated animals. One day after cell transfer, we administered MOG_{35-55} in CFA + PTX to induce EAE. We saw a significant reduction in the mean clinical EAE score in mice that received splenocytes from mice treated with VHH_{MHCII}-MOG_{35-55} (Fig. 2b, Supplementary Fig. 8). We eliminated macrophages and CD8 T cells *in vivo* by administering the corresponding depleting antibodies: anti-CFS1R antibodies and anti-CD8a antibodies respectively (Fig. 2c, Supplementary Fig. 9) [15]. To deplete DCs, we administered diphtheria toxin (DTX) in CD11c-DTR (diphtheria toxin receptor) mice (Fig. 2c, Supplementary Fig. 9) [16]. To test the possible involvement of B cells, we administered VHH_{MHCII}-MOG_{35-55} into mMt-/- mice, which lack mature B cells [17]. Only elimination of CD11c+ DCs reduced the measure of protection provided by VHH_{MHCII}-MOG_{35-55} (Fig. 2c, Supplementary Fig. 9). We created two VHH-MOG_{35-55} adducts that presumably target different but overlapping subsets of myeloid cells: we used a VHH directed against CD11b (mostly present on macrophages) and a VHH that recognizes CD11c (mostly present on dendritic cells) (Supplementary Fig. 1) [7]. Only the VHH_{CD11c}-MOG_{35-55} combination provided an intermediate level of protection against the induction of EAE (Fig. 2d, Supplementary Fig.10), consistent with the results from elimination of CD11c+ cells. Batf3-/- mice treated with VHH_{MHCII}-MOG_{35-55} remained resistant to the induction of EAE [18]. In this setting CD8a+ DCs therefore do not contribute to the set of tolerogenic APCs (Supplementary Fig. 11).

To determine whether delivery by VHH_{MHCII} of more than just the minimal epitope can likewise induce tolerance, we generated VHH_{MHCII}-MOG_{17-78} and treated mice 7 days prior to challenge (Fig. 2e). VHH_{MHCII}-MOG_{17-78} likewise protected against induction of EAE (Fig. 2f). This shows that our approach can tackle a condition where the offensive protein but not its minimal epitope(s) is known.

Administration of VHH_{MHCII}-MOG_{35-55} elicits a burst of proliferation, followed by attrition, of MOG_{35-55}-specific CD4 T cells. To investigate the impact of VHH_{MHCII}-MOG_{35-55} adducts on T cells of defined antigen specificity we used 2D2 TCR transgenic mice as a source of monoclonal CD4+ T cells that

recognize the I-A^b- MOG_{35-55} complex [19]. We transferred congenically marked, Violet CellTrace-labeled 2D2 CD45.2+ CD4+ T cells into CD45.1 recipients, followed by injection i.v. of VHH_{MHCII}-peptide adducts one day later. We tracked the number of 2D2 cells in spleen, inguinal lymph nodes (iLNs), and blood for 10 days. In mice receiving VHH_{MHCII}-MOG_{35-55}, 2D2 CD4+ T cells underwent an initial burst of expansion, followed by contraction on day 5 post-injection, as judged from the absolute number of 2D2 cells recovered from spleen, iLNs, and blood as well as whole body imaging using non-invasive positron emission tomography (PET) for CD4+ cells (Fig. 3a, Supplementary Fig. 12). Such disappearance occurred after several divisions: all of the recovered 2D2 CD4+ T cells were antigen-experienced and had divided, as evident from Violet CellTrace dilution (Fig. 3b). Delivery of an amount of MOG_{35-55} equimolar to that of the administered VHH_{MHCII}-MOG_{35-55} adduct led to division of no more than ~5% of the 2D2 T cells. VHH_{MHCII}-mediated antigen delivery thus clearly enhances its presentation (Fig. 3b).

MOG-specific 2D2 CD4 T cells upregulate co-inhibitory receptors upon administration of VHH_{MHCII}-MOG_{35-55}. We next examined the transcriptome of 2D2 T cells in VHH_{MHCII}- MOG_{35-55} recipients. We sorted 2D2 CD4 T cells at different divisional stages (Fig. 3b) and performed RNAseq analyses. Injection of VHH_{MHCII}-MOG_{35-55} upregulates co-inhibitory receptor transcripts as well as negative regulatory transcription factors. LAG3 transcripts stand out in both magnitude and significance (Fig. 3c, d, Supplementary Fig. 13). At the protein level, these 2D2 T cells also showed higher levels of apoptotic and exhaustion markers, such as PD1 and LAG3, but not Tim3, Fas/CD95, or LAP (Fig. 3e, Supplementary Fig. 14) [20]. At day 3 post-injection, 2D2 CD4 T cells in VHH_{MHCII}-MOG_{35-55} recipients failed to down-regulate CD62L, while remaining CD44+ (Supplementary Fig. 14). When we treated LAG3-/- mice with a single dose of VHH_{MHCII}-MOG_{35-55} and then attempted to induce EAE, protection was lost, albeit with significant delay, whereas PD1-/- mice were still tolerized by VHH_{MHCII}-MOG_{35-55} (Fig. 3f). Deletion of LAG3 in 2D2 TCR transgenic mice has been shown to cause spontaneous EAE [21]. This indicates the importance of LAG3 pathway in this tolerance induction strategy.

Because both activated effector T cells and Tregs express LAG3, we then evaluated whether an increase in regulatory T cells contributes to VHH_{MHCII}-MOG_{35-55}-imposed tolerance [22]. To uncover a role for regulatory T cells in VHH_{MHCII}-MOG_{35-55}-mediated tolerance, we eliminated Tregs in Foxp3-DTR mice by administration of DTX (Supplementary Fig. 15) [23]. Treated mice lost Tregs and were no longer protected against EAE, demonstrating their contribution to VHH_{MHCII}-MOG_{35-55}-imposed tolerance (Supplementary Fig. 15). Administration of VHH_{MHCII}-MOG_{35-55} increases the number of FoxP3+ MOG_{35-55}-specific Tregs (Supplementary Fig. 15).

Finally, we challenged mice that had received 2D2 T cells with MOG_{35-55}/CFA at day 10. The 2D2 T cells in mice that received VHH_{MHCII}-MOG_{35-55} failed to respond, whereas 2D2 T cells in mice injected with VHH_{MHCII}-$OVA_{323-339}$ proliferated robustly (Fig. 3g). This underscores the antigen specificity of tolerance induction by VHH_{MHCII}-MOG_{35-55}.

VHH_{MHCII}-antigen adducts act in an antigen-specific manner in other models of autoimmunity. We next explored other examples of autoimmunity. For type-1 diabetes (T1D), we used the aggressive BDC2.5 T cell adoptive transfer model, which mimics destruction of β-cells by autoreactive T cells. TCR transgenic CD4 T cells that carry the BDC2.5 T cell receptor recognize pancreatic β cells and can be activated *ex vivo* with a 10-residue peptide, the mimotope p31. In NOD/SCID mice, such activated BDC2.5 T cells cause hyperglycemia within 8 days after transfer [24]. We conjugated p31 to VHH_{MHCII} (Supplementary Fig. 1). NOD/SCID mice that received activated BDC2.5 splenocytes were treated a day later with either saline, 20mg VHH_{MHCII}-MOG_{35-55}, or 20mg VHH_{MHCII}-p31 (Fig. 4a). Only mice treated with VHH_{MHCII}-p31 remained normoglycemic (Fig. 4a, Supplementary Fig. 16). VHH_{MHCII}-p31-treated mice had fewer BDC2.5 CD4 T cells in their pancreas and secondary lymphoid organs (Supplementary Fig. 16). Islets in protected mice remained intact (Fig. 4b). We saw a mild protective effect even when we administered VHH_{MHCII}-p31 to mice relatively late, on day 5 post-transfer of the activated BDC2.5 T cells (Supplementary Fig. 16).

Arthritis can be induced in BALB/c recipients by intravenous transfer of *ex vivo* activated DO11.10 T cells that recognize $OVA_{323-339}$, followed one day later by re-stimulation *in vivo* with a footpad injection of OVA/CFA emulsion and a challenge 10 days later by injection of heat-aggregated ovalbumin (Fig. 4c) [25]. Mice were monitored for development of arthritis by measuring paw thickness and by histological assessment at day 7 following a challenge with heat-aggregated ovalbumin. Prior administration of VHH_{MHCII}-$OVA_{323-339}$ reduced joint inflammation upon exposure to ovalbumin, whereas VHH_{MHCII}-MOG_{35-55} had no effect (Fig. 4c, Supplementary Fig. 17). Mice treated with VHH_{MHCII}-$OVA_{323-339}$ showed fewer signs of cartilage destruction (Fig. 4d). Immune cells obtained from popliteal lymph nodes of mice treated with VHH_{MHCII}-$OVA_{323-339,}$ when stimulated *ex vivo* with OVA, failed to produce IFNg (Supplementary Fig. 17). Perhaps not unexpectedly, serum from mice treated with VHH_{MHCII}-$OVA_{323-339}$ also had lower levels of anti-OVA and anti-$OVA_{323-339}$ IgG1 antibodies (Supplementary Fig. 17). Combined, these results confirm the ability of VHH_{MHCII}-antigen adducts to reduce the harm inflicted by activated, autoreactive CD4 T cells. The underlying mechanism(s) must be conserved across mouse MHC haplotypes.

VHH_{MHCII}-antigen adducts also suppress CD8 T and B responses. To determine whether CD8 T cell responses are affected by administration of VHH_{MHCII}-antigen adducts, we attached the OVA-derived CD8 T cell epitope SIINFEKL (the OTI peptide restricted by H-$2K^b$) to VHH_{MHCII} (Supplementary Fig. 1) [26]. Mice received congenically marked OTI T cells, followed by injection of VHH_{MHCII}-OTI or VHH_{MHCII}-ORF8 (with or without adjuvant) a day later (Fig. 4e). The ORF8 epitope derived from MCMV is recognized by CD8 T cells in H-2^b mice and served as a control [27]. A re-challenge of the recipients with OVA/CFA at day 10 post transfer failed to activate any remaining OTI T cells (Figs. 4e, f). To explore whether B cell responses are similarly affected by administration of VHH_{MHCII}-antigen adducts, we modified VHH_{MHCII} with a B cell-specific OVA-derived epitope (OB1) (Supplementary Fig. 1) [28]. Three consecutive injections of VHH_{MHCII}-OBI into C57BL/6J recipients failed to elicit IgG antibody responses against either intact OVA

protein or the OB1 peptide (Figs. 4g, h), whereas mice that received equimolar amounts of free OVA protein readily produced such antibodies.

Co-delivery of VHH_{MHCII}-MOG_{35-55} and VHH_{MHCII}-dexamethasone improves therapeutic efficacy. We then explored the impact of VHH_{MHCII}-MOG_{35-55} administration to mice already symptomatic for EAE. Injection of VHH_{MHCII}-MOG_{35-55} into mice that had developed an EAE score of 1 (limp tail) halted progression of EAE in 9 out of 16 mice (Fig. 5a, Supplementary Fig. 18). For the remaining 7 out of 16 mice, their overall condition rapidly deteriorated (shivering; reduced motor activity) after injection of VHH_{MHCII}-MOG_{35-55}, seemingly unrelated to EAE. A cytokine storm elicited by the targeted delivery of antigen into an already inflamed environment was responsible (Fig. 5c). The polyclonal nature of the evoked T cell response and the rather superficial clinical scoring system imply heterogeneity in the diseased cohort, which may explain why not all animals that received VHH_{MHCII}-MOG_{35-55} responded similarly. We wondered whether it might be possible to co-deliver an immunosuppressive drug to avert a cytokine storm. We delivered the immunosuppressive corticosteroid dexamethasone, attached via a self-immolating hydrazone linker to VHH_{MHCII}, to Class II MHC+ cells (VHH_{MHCII}-DEX; Fig. 5b, Supplementary Fig. 19) [29]. Mice that received a combined dose of 20mg VHH_{MHCII}-MOG_{35-55} and 20mg VHH_{MHCII}-DEX survived and reverted to lower clinical EAE clinical scores, without obvious side effects (Fig. 5d). Improvements in clinical score were mirrored by a reduction in infiltrating CD4 T cells in the spinal cord (Supplementary Fig. 20). The observed benefit required no more than the equivalent of 0.5mg DEX in the form of the VHH_{MHCII}-DEX adduct. Free DEX, on the other hand, provided protection only when administered at a ~200-fold higher dose of 100mg i.p. (Supplementary Fig. 21). We extended the therapeutic range to animals that had progressed to an EAE score of 2 or 3, all of which responded to co-administration of VHH_{MHCII}-MOG_{35-55} and VHH_{MHCII}-DEX by an arrest in disease progression, again without side effects. Affected mice even showed a significant amelioration in disease score (Figs. 5e, f, Supplementary Fig. 20).

Discussion

Various modes of antigen delivery can induce antigen-specific tolerance in pre-clinical models of autoimmune disease, with some promise in early-stage clinical trials [30]. Drastic immune ‘resetting’ by myeloablation, followed by autologous hematopoietic stem cell transplantation, has produced promising results in severely ill patients with myasthenia gravis and multiple sclerosis [31]. Other cell-based therapies include transfusion of modified immune cells, including dendritic cells and engineered erythroid cells [32-35]. Tolerogenic nanoparticles have also been explored as a means of intervention in autoimmunity [36, 37]. In addition to curbing inflammation, wholesale immunosuppression is the backstop in the treatment of autoimmunity, a therapy that can increase the risk of infectious disease. While antibiotic treatment can mitigate this drawback at least in part, the search for a more targeted approach to blunt undesirable immune reactions remains a priority.

The induction of antigen-specific tolerance is a particularly high bar to clear if one considers the presence of pathology and pre-existing autoimmunity at diagnosis. Autoimmune destruction of target cells predates the onset of symptoms that bring the patient to medical attention. Therapy must therefore deal not only with pre-existing autoimmunity but also with the possibility of epitope spreading beyond the initiating insult. Any type of prophylactic treatment will be of limited use unless susceptible populations can be identified unambiguously, and then only if the risk of eliciting unwanted side effects of the proposed treatment is acceptably small.

The recent and rather narrow focus on dendritic cells as a key component of cell-based interventions in immunity has overshadowed earlier work in which antigens were targeted to Class II MHC products, expressed on all antigen presenting cells [5, 38, 39]. This was done through the creation of full-size anti-Class II MHC monoclonal antibodies conjugated to antigens to elicit an immune response. For this reason, we chose to deliver nanobody-autoantigen fusions under non-inflammatory conditions to MHCII+ cells, a strategy that does not obviously differentiate among the various APC subsets, but is efficacious, nonetheless. More importantly, our anti-mouse VHH_{MHCII} does not distinguish between MHCII allotypes. We showed that it is not essential to deliver the minimal CD4 T cell epitope, but that larger fragments can also lead to tolerogenic antigen processing and presentation (Figs. 2e, f). Depending on the size of the autoantigen, VHH_{MHCII}-antigen adducts can eliminate the need for precise epitope identification in a disease or protein replacement setting. This highlights advantages of the approach reported here, successful in the prevention of autoimmunity in three mouse models, over those that employ defined allotypes of Class II MHC molecules complexed with relevant antigenic epitopes [40]. Ideally, interventions ought to be antigen-specific and as simple as possible, both from a manufacturing and application perspective. The VHH_{MHCII} adducts described here meet that criterion. We hypothesize that antigen delivery to Class II MHC+ cells cover the relevant tolerogenic APCs and obviates the need of identifying disease-specific or organ specific APCs.

In conclusion, a MOG_{35-55}-modified VHH that recognizes Class II MHC products can protect mice against the induction of EAE. A single injection of 20mg of the VHH_{MHCII}-antigen adduct affords protection that lasts for at least two months. Administration of the same VHH_{MHCII}-MOG_{35-55} adduct in animals that already show symptoms of EAE (score 1, 2 or 3) halts progression and even allows partial reversal of the severity of the symptoms. Only a subset of animals symptomatic for EAE responded to treatment with VHH_{MHCII}-MOG_{35-55} without undesirable side effects, whereas the remainder showed rapid exacerbation attributable to a cytokine storm. An inflammatory environment must already exist in symptomatic animals, such that delivery of the VHH_{MHCII}-MOG_{35-55} adduct to APCs only adds fuel to the fire. Indeed, administration of nanobody-peptide adducts in the presence of anti-CD40 and poly dIdC as adjuvants strongly potentiates antibody responses against them [7]. To overcome this acute response, we co-delivered a VHH_{MHCII}-dexamethasone adduct, which rescued survival. In a setting where there is a chronic inflammatory response, administration of the type of nanobody adducts developed here would be possible only if appropriate supporting measures were available, as in the case of the VHH_{MHCII}-dexamethasone adduct.

The pharmacokinetic properties of nanobodies make them particularly attractive for the construction of antibody-drug conjugates (ADCs) [41, 42]. Full-sized immunoglobulin-based ADCs continue to circulate for periods up to weeks and release payloads directly into the bloodstream upon hydrolysis of the linkers via which the drugs are attached. This can result in unwanted systemic drug exposure. In contrast, the VHH_{MHCII}-dexamethasone adduct has the desired properties of excellent targeting, as verified by non-invasive imaging, short circulatory half-life and ease of modification [43]. The cellular targets recognized by VHH_{MHCII} include all MHCII+ cells. Even if the types of APC responsible for induction of tolerance and for provoking a cytokine storm are several and distinct, the MHCII-based targeting approach would cover them. Nanobody-drug adducts have yet to find the broad range of applications of their full-sized counterparts, but our data show it is an opportunity not to be discounted and pointed to the immense potential of our method.

Methods

Expression of VHHs and endotoxin removal

WK6 *E. coli* containing the plasmid encoding corresponding VHHs were grown to mid-log phase at 37°C in Terrific Broth plus ampicillin and induced with 1 mM IPTG overnight at 30°C. Bacteria were harvested by centrifugation at 5,000g for 15 minutes at 4 °C and then resuspended in 25 mL 1× TES buffer (200 mM Tris, pH 8, 0.65 mM EDTA, 0.5 M sucrose) per liter culture and incubated for 1 hour at 4 °C with agitation. Resuspended cells were then submitted to osmotic shock by 1:4 dilution in 0.25× TES buffer and incubation overnight at 4 °C. The periplasmic fraction was isolated by centrifugation at 5,000g for 30 min at 4 °C and then loaded onto Ni-NTA (Qiagen) in 50 mM Tris, pH 8, 150 mM NaCl, and 10 mM imidazole. Protein was eluted in 50 mM Tris, pH 8, 150 mM NaCl, 500 mM imidazole, and 10% glycerol and then loaded onto a Superdex 75 10/ 300 column in 50 mM Tris, pH 8, 150 mM NaCl, 10% glycerol. The peak fractions were recovered and rebounded to Ni-NTA to be depleted of LPS (<2 IU/mg). Bound VHHs were washed with 40 column volumes of PBS + 0.1% TritonX-114 and eluted in 2.5 column volumes endotoxin-free PBS (Teknova) with 500 mM imidazole. Imidazole was removed by PD10 column (GE Healthcare), eluting in LPS-free PBS. Recombinant VHH purity was assessed by SDS/PAGE and LC-MS.

Chemical Synthesis of GGG-antigens, GGG-Cy5 and GGG-DEX

The peptides were synthesized on 2-Chlorotrityl resin (ChemImpex) following standard solid phase peptide synthesis (SPPS) protocol or ordered on GenScript. For GGG-Cy5, GGGC (7.0 mg, 24 µmol) was dissolved in DMSO (Sigma Aldrich) (400 µL) and was added to Cyanine 5 maleimide (Lumiprobe) (5.0 mg, 7.8 µmol). The resulting mixture was gently agitated at room temperature until LCMS analysis show no remaining starting material. The ligated product was then purified by RP-HPLC and lyophilized. LC-MS calculated for GGG-Cy5: $C_{47}H_{62}N_8O_8S_2$ [M+H]+ was 898.44, found 898.56. The resulting powder was stored at 4ºC.

For GGG-Dexamethasone (DEX), in the first reaction, dexamethasone (Sigma Aldrich) (25 mg, 64 µmol) and N-β-maleimidopropionic acid hydrazide (ThermoFisher) (40 mg, 135 µmol) was dissolved in 3.0 mL of dry MeOH (Sigma Aldrich) and one drop of TFA was added to the solution. The resulting mixture was agitated overnight at room temperature. The MeOH was then evaporated, the precipitate dissolved in DMSO (1.0 mL), purified by RP-HPLC and lyophilized. LC-MS calculated for DEX-maleimide: $C_{29}H_{37}FN_3O_7$ [M+H]+ was 558.26, found 558.32. The resulting powder was stored at -20 ºC. In a second reaction, DEX-maleimide (20 mg, 36 mol) and GGGC (21 mg, 72 µmol) were dissolved in 5% 0.1 M $NaHCO_3$ in DMSO (1.0 mL). The resulting mixture was agitated at room temperature until completion of the reaction. Once no starting material was left, the reaction was directly purified by RP-HPLC and lyophilized. LC-MS calculated for GGG-DEX: $C_{38}H_{53}FN_7O_{12}S$ [M+H]+ was 850.35, found 850.21. The resulting peptide was stored at -20 ºC and re-dissolved in PBS before at the right concentration before sortase ligation.

C-terminal sortagging of VHH-LPETGG or GFP-LPETGG with GGG-carrying moieties

Reaction was carried out in 1 mL mixture containing Tris·HCl (50 mM, pH 7.5), CaCl2 (10 mM), NaCl (150 mM), triglycine-containing probe (500 µM), GGG-containing probe (100 µM), and 5M-Sortase A (5 µM). After incubation at 4°C with agitation for 1.5 hours, unreacted VHH and 5M-SrtA were removed by adsorption onto Ni-NTA agarose beads. The unbound fraction was concentrated and excess nucleophile with an Amicon 3,000 KDa MWCO filtration unit (Millipore). Reaction products were analyzed by LC-MS for purity and stored at −80°C.

Mice

All animals were housed in the animal facility of Boston Children's Hospital (BCH) and were maintained according to protocols approved by the BCH Committee on Animal Care. C57BL/6J (CD45.2+), B6.SJL-Ptprc (CD45.1+), NOD/SCID, BALB/c, B6/2D2, NOD/BDC2.5, BALBC/DO11.10, CD11c-DTR, µMT-/-, Batf3-/-, LAG3-/-, and FoxP3-DTR mice were either purchased from the Jackson Laboratory or bred in house. MHCII-GFP and PD1-/- mice were bred in house. OTI Rag2-/- mice were purchased from Taconic.

Flow Cytometry Analyses

Cells were harvested from spleen, lymph nodes, or other organs and were dispersed into RPMI1640 through a 40-micron cell strainer using the back of a 1 mL syringe plunger. Cell mixture were subjected to hypotonic lysis (NH_4Cl) to remove red blood cells, washed twice in FACS buffer (2 mM EDTA and 1% FBS in PBS) and resuspended in FACS buffer containing the corresponding fluorescent dye–conjugated antibodies. All staining was carried out at 1:100 dilution and with Fc block for 30 min at 4°C in dark. Samples were washed twice with FACS buffer before further analysis. All flow data were acquired on a FACS Fortessa flow cytometer (BD Biosciences) and analyzed using FlowJo software (Tree Star).

The following is the list of antibodies used in this study:

Target	Color	Clone	Manufacturer	Cat. Number
B220	Alexa 700	RA3-6B2	eBioscience	56-0452-82
CD115(CSF1R)	PeCy7	AFS98	Biolegend	135523
CD11b	APC	M1/70	Biolegend	101212
CD11b	BV711	M1/70	Biolegend	101242
CD11c	PerCP	N418	BioLegend	117326
CD11c	BV605	N418	Biolegend	117333
CD19	PE	6D5	Biolegend	115508
CD27	APC-Cy7	LG.3A10	Biolegend	124225
CD3	BV421	17A2	Biolegend	100228
CD4	FITC	GK1.5	Biolegend	100406
CD4	APC	RM4-5	Biolegend	100516
CD4	PeCy7	RM4-5	Biolegend	100528
CD44	PE	IM7	Biolegend	103008
CD45.1	PeCy7	A20	eBioscience	25-0453-82
CD45.2	APC	104	Biolegend	109814
CD45.2	PeCy7	104	Biolegend	109830
CD5	PE	53-7.3	Biolegend	100607
CD62L	PeCy7	MEL-14	Biolegend	104418
CD8	APC-Cy7	53-6.7	BioLegend	100714
CD95	PeCy7	Jo2	BD Bioscience	557653
Fc block (CD16/CD32)	N.A.	93	Biolegend	101302
FoxP3	eFluor 450	FJK-16s	eBioscience	2136519
FoxP3	FITC	FJK-16s	Invitrogen	430671
IFNγ	FITC	XMG1.2	Biolegend	505806
IgD	BV711	11-26c.2a	Biolegend	405731
IL17a	PE	TC11-18H10.1	Biolegend	506904
Lag3 (CD223)	PE	eBioC9B7W	eBioscience	12-2231-81
LAP	PE	TW7-16B4	BD Bioscience	563143
MHC Class II (I-A/I-E)	PE	M5/114.15.2	Biolegend	107608
PD1 (CD279)	PeCy7	29F.1A12	Biolegend	135216
PDCA-1 (CD317)	PE	129C1	Biolegend	127103
TCRa3.2	APC	RR3-16	Invitrogen	17-5799-82
TCRb11	PerCP-eFluor 710	RR3-15	eBioscience	46-5827-80
Tim-3 (CD366)	PE	RMT3-23	Biolegend	119704

Experimental Autoimmune Encephalomyelitis (EAE) Model in C57BL/6J mice

Female C57BL/6 mice (10–12 weeks of age) or other mouse lines with C57BL/6J genetic background were immunized with Hooke kits: an emulsion of MOG_{35-55} in CFA and PTX in PBS according to the manufacturer's instructions (Hooke laboratories). Mice were scored daily, starting on day 7 post-immunization by an investigator blinded to the experimental treatment of individual mice. Mice were assigned to different experimental treatments randomly and cohoused together to eliminate inter-cage variability. All treatments were carried out on at least 3 mice and in at least two independent experiments,

as indicated in the figure legends. All animals were included in the analyses. Clinical score is defined as follows: 1, limp tail; 2, partial hind leg paralysis; 3, complete hind leg paralysis; 4, complete hind and partial front leg paralysis; and 5, moribund. Easy access to wet food and water was provided for the experimental mice throughout the disease progression. Unless indicated otherwise, for prophylactic treatment, 20mg sortagged VHH-antigens were intravenously administered 7 days prior to induction of EAE. For therapeutic treatment, 20mg VHH_{MHCII}-$OVA_{323-339}$, VHH_{MHCII}-MOG_{35-55}, or 20mg VHH_{MHCII}-MOG_{35-55} mixed 20mg VHH_{MHCII}-DEX were administered on the day of EAE when the mice exhibited symptoms defined as clinical score of 1, 2, and 3 as indicated. At day 30 post-EAE induction or when mice reached clinical score of 4, mice were sacrificed by asphyxiation and then perfused with 5 mM EDTA in PBS. Spinal cords were isolated and fixed in 10% (wt/vol) formalin solution (Sigma), embedded in paraffin, sectioned at 20µm, and stained with H&E or Luxol Fast Blue (Harvard Medical School Rodent Histology Core Facility). Stained sections were imaged at 4× and 10× magnification. Isolation of the immune cells that infiltrate the spinal cord was carried out by homogenizing the spinal cord, followed by 38% Percoll (Sigma) gradient separation (100% Percoll is 1.123 g/mL). Isolated cells were plated in 48-well plates and treated with 50ng/mL PMA (Sigma) and 500ng/mL ionomycin (Sigma) for 2 hours at 37°C in complete RPMI media, followed by the addition of 10µg/mL Monensin (Sigma) and incubated for 2 more hours. Cells were then surface stained, fixed, and permeabilized using Foxp3/Transcription Factor Staining Buffer Set (ThermoFisher Scientific, 00-5523-00) according to the manufacturer's protocol. Intracellular and Foxp3 staining were performed according to the manufacturer's protocols and cell samples were then used for flow cytometry.

For cytokine storm analysis, blood samples were taken 6 hours post therapeutic treatment with 20 mg VHH_{MHCII}- MOG_{35-55}, VHH_{MHCII}-$OVA_{323-339}$, or 20 mg VHH_{MHCII}-MOG_{35-55} + 20 µg VHH_{MHCII}-DEX on the first day these EAE mice reached clinical score of 3. Blood was collected in EDTA containing tubes and plasma was isolated via repeated centrifugation (500g, 5 min, 4°C). Plasma was stored at -80 °C until further analysis of tumor necrosis factor alpha (TNF-α) and interleukin 6 (IL-6). TNF-α (ThermoFisher, 88-7324-22) and IL-6 (ThermoFisher, 88-7064-22) ELISAs were conducted according to manufacturer's protocol.

Cellular subset depletion

CD8 T cells were depleted by administering 400mg of anti-CD8α depleting antibody (clone 2.43, BioXCell) intraperitoneally twice weekly beginning 2 weeks prior to prophylactic treatment with VHH-antigen and throughout the EAE observation window. Macrophage subsets were ablated by injecting 300mg anti-CSF1R (clone AFS98, BioXCell) every other day from 2 weeks prior to prophylactic treatment up to the end of the experimental set up. To deplete DCs, we administered 100ng DTX (Sigma) intraperitoneally into CD11c-DTR mice 2 days prior to VHH-antigen administration. For depleting Tregs, FoxP3-DTR mice were injected with 3 doses of 1mg DTX (Sigma) intraperitoneally at day -9, -8, and -1 prior to prophylactic treatment with VHH-antigen and weekly afterwards until the end of observation window. Cellular depletions were confirmed by flow cytometry of PBMCs or splenocytes.

2D2 CD4 T-Cell Adoptive Transfer and Challenge

Splenic and iLNs-derived CD4 T cells from 2D2 mice were enriched by negative selection using magnetic beads (Miltenyi Biotec, 130-104-453) and labeled with Violet CellTrace (ThermoFisher Scientific, C34571) as per the manufacturer's protocol. 500,000 of these 2D2 CD4+ T cells were transferred into CD45.1+ mice. Transfusion of 20mg VHH_{MHCII}-$OVA_{323-339}$, 20mg VHH_{MHCII}-MOG_{35-55}, equimolar of MOG_{35-55} peptides, or 100mg MOG_{35-55} peptides mixed with 25mg anti-CD40 (SouthernBiotech) and 50mg PolyI:C (Sigma) as adjuvant was carried out the day after adoptive transfer. At day 3, 5, and 10, mice were sacrificed and spleens, iLNs, and blood were collected and analyzed by flow cytometry. Some of these 2D2 T cell adoptively transferred mice were also challenged on day 3 or 10 with 100mg MOG_{35-55} in CFA subcutaneously. Mice were sacrificed 7 or 5 days later as indicated in the respective experimental set up. Spleens, iLNs, and blood were harvested and analyzed by flow cytometry.

2D2 CD4 T Cell RNAseq

Cells were sorted and lysed in RLT lysis buffer (Qiagen) supplemented with n-mercaptoethanol. RNA was the isolated using a RNeasy Micro kit (Qiagen) according to the manufacturer's protocol. 20ng of RNA were used as input to a modified SMART-seq2 protocol. The resulting library was confirmed using a High Sensitivity DNA Chip run on a Bioanalyzer 2100 system (Agilent), followed by library preparation using the Nextera XT kit (Illumina) and custom index primers according to the manufacturer's protocol. Final libraries were quantified using a Qubit dsDNA HS Assay kit (Invitrogen) and a High Sensitivity DNA chip run on a Bioanalyzer 2100 system (Agilent). All libraries were sequenced using Nextseq High Output Cartridge kits and a Nextseq 500 sequencer (Illumina). Sequenced libraries were demultiplexed using the bcl2fastq program and the resulting Fastq data were trimmed and cropped with Trimmomatic. Alignment to the mouse mm10 reference genome and gene expression counts were carried out using Kallisto. Principal Component Analyses (PCA) were carried out in R. To test for differential gene expression from our RNA-seq data and differential chromatin accessibility in individual loci, we used the DEseq2 method. Volcano plot and heatmaps were generated in Python 3.6 using NumPy 1.12.1, and Matplotlib 2.2.2. For functional analyses, Gorilla (Gene Ontology Enrichment Analysis and Visualization Tool) was used to find enriched Gene Ontology (GO) terms in the up-regulated and down-regulated subsets of the top 500 most differentially expressed genes. The datasets generated during the current study are available from the corresponding author on reasonable request.

Type 1 Diabetes (T1D) Model in NOD/SCID mice

Spleen and inguinal lymph nodes were harvested from 7-9-week-old BDC2.5 mice. Cells were resuspended in complete RPMI (RPMI supplemented with 2mM glutaMAX, 10 mM HEPES, Non-Essential Amino Acids, 1 mM Sodium pyruvate, 55uM 2-mercaptoethanol, 10% heat-inactivated FBS) supplemented with 0.5 mM p31 peptide (BDC2.5 mimotope, GenScript) and plated in tissue culture dishes at 1 million cells/mL. After four days, cells were harvested, washed twice and resuspended in PBS. 5 million cells were adoptively transferred into 9-12-week-old female NOD.SCID mice via retro-orbital

injection. Saline, 20mg VHH_{MHCII}-p31, or VHH_{MHCII}-MOG_{35-55} were infused into the mice a day or 5 days later as indicated. Blood glucose measurements were carried out every other day for 2 weeks and weekly for up to 1-2 months. Mice were considered diabetic when their blood glucose level exceeded 260 mg/dL for two subsequent weeks as measured by using the Active meter (Accu-Chek) (range 20-600 mg/dL) with corresponding Aviva Plus test strips (Accu-Check).

Mice were sacrificed via asphyxiation at the 2-month endpoint or when blood glucose levels exceeded 600 mg/dL for two subsequent weeks. The pancreas was fixed for further immunohistochemistry analysis, i.e. H&E staining (Harvard Medical School Rodent Histology Core Facility). In a separate cohort of mice, spleens, inguinal/pancreatic lymph nodes and pancreas were harvested at day 14 post adoptive transfer for flow cytometry analysis.

Rheumatoid Arthritis (RA) Model in BALB/c mice

Spleen and lymph nodes were collected from DO11.10 mice. CD4+ T cells from these mice were enriched by negative selection using magnetic beads (Miltenyi Biotec, 130-104-453). We also obtained APCs by irradiating DO11.10 splenocytes at 2000rad. We induce the differentiation of these naïve CD4 T cells into Th1 phenotypes by culturing them as follows: 200,000 CD4+ T cells and 2 millions APCs were co-cultured in complete RPMI containing 0.3mM $OVA_{323-339}$ (GenScript), 5ng/mL IL12 (PeproTech), and 10mg/mL anti-IL4 mAb (R&D Systems) for 3 days. Cells were then harvested, washed, and counted. A total of 2 millions Th1 DO11.10 T cells were injected intravenously into BALB/c recipients. One day following T cell transfer, recipients were immunized subcutaneously with 100mg OVA in CFA (Sigma-Aldrich). At day 11, we injected heat aggregated OVA (HOA) into the left paw of the mice and measure their paw thickness daily up to day 18. Mice were then sacrificed, and their paws were removed and fixed in 10% (wt/vol) formalin solution (Sigma), embedded in paraffin, sectioned at 20mm, and stained with Toluidine Blue (Harvard Medical School Rodent Histology Core Facility). Stained sections were imaged at 4× and 10× magnification. We also collected popliteal lymph nodes and restimulate the cells in vitro with 1mg/mL OVA in complete RPMI for 3 days for IFN-γ production. IFNγ was measured using the Mouse IFN-γ ELISA Set (BD Biosciences, 555138) per manufacturer's protocol. Sera was also collected at D18 end point for ELISA assays to measure anti-OVA and anti-$OVA_{323-339}$ antibody responses. 96-well plates were coated with 10 mg/mL of OVA or GFP-$OVA_{323-339}$ (generated by sortagging GFP-LPETGG with GGG-$OVA_{323-339}$) proteins in PBS overnight at 4°C and incubated in blocking buffer (0.05% Tween20 + 2% BSA in PBS) before addition of serum samples. Incubation with tested serum was for 3 hours at room temperature. Plates were washed four times with PBS, incubated with goat anti-mouse IgG-HRP (SouthernBiotech) at 1:10,000 in blocking buffer for 1 hour, and developed with 3,3',5,5'-Tetramethylbenzidine (TMB) liquid substrate reagent (Sigma). The reaction was stopped with 1 N HCl and absorbance was read at 450nm.

OTI CD8 T-Cell Adoptive Transfer and Challenge

Spleen and lymph nodes were collected from OTI Rag2−/− mice. CD8+ T cells from OTI Rag2−/− were enriched by negative selection using magnetic beads (Miltenyi Biotec, 130-095-236) and labeled with

Violet CellTrace as the manufacturer's protocol. 500,000 CD8+ T cells were transferred intravenously into CD45.1+ mice. Transfusions of 20mg VHH_{MHCII}-OTI or VHH_{MHCII}-ORF8 were carried out the day after adoptive transfer. Mice were challenged on day 10 with 25mg OTI peptide in CFA (Sigma) and then sacrificed 5 day later for analyses. Spleens, iLNs, and blood were harvested and splenocytes were analyzed by flow cytometry.

Two million splenocytes were plated in 96-well round-bottomed plates and treated with Cell Stimulation Mixtures (eBioscience) and Brefeldin A (eBioscience) for 3 days at 37 °C in complete RPMI [RPMI 1640, 10% (vol/vol) heat-inactivated FBS, 50 mM β-mecaptoethanol, 100 U/mL Pen/Strep, 1× Gibco MEM NonEssential Amino Acids Solution (Life Technologies), 1 mM Sodium pyruvate, 1 mM Hepes] supplemented with 1mg/mL OVA peptides. Supernatant was collected and utilized for ELISA to measure Interferon gamma (IFNγ) production. IFNγ was measured using the Mouse IFN-γ ELISA Set (BD Biosciences, 555138) per manufacturer's protocol.

Repeated Transfusions of VHH_{MHCII}-OB1

OB1 is a 17-mer B cell epitope derived from OVA. C57BL6/J recipient mice were intravenously injected with 20μg VHH_{MHCII}-OB1, equimolar amount of OVA proteins, or PBS at day 0. Subsequent boosts were carried out on day 7 and day 14. Serum samples were collected pre-immunization and 7 days after the last boost. For OVA-specific and OB1 peptide-specific ELISA, 96-well plates were coated with 10 μg/mL of OVA or GFP-OB1 proteins in PBS overnight at 4°C and incubated in blocking buffer (0.05% Tween20 + 2% BSA in PBS) before addition before addition of serum samples. Incubation with tested serum was for 3 hours at room temperature. Plates were washed four times with PBS, incubated with goat anti-mouse IgG-HRP (SouthernBiotech) at 1:10,000 in blocking buffer for 1 hour, and developed with 3,3',5,5'-Tetramethylbenzidine (TMB) liquid substrate reagent (Sigma). The reaction was stopped with 1 N HCl and absorbance was read at 450 nm.

Statistical Methods

All data represented at least two independent experiments. All statistical analyses were performed using Prism 6. Statistical methods used are indicated in the corresponding legend of each figure. Statistically significant differences are indicated by asterisks as follows: ***p < 0.001.

Declarations

Acknowledgements

This work is supported by Junior Fellowship from Harvard Society of Fellows (to N.P.), Postdoc. Mobility fellowship from the Swiss National Science Foundation (SNSF), grant number P400P2_183857 (to T. J. H.), a scholarship from the Dutch MS Research Foundation (to L.Y.S and R.J.), the overseas grant from UiT The Arctic University of Norway (to A. I.), and the NIH Director's Pioneer Award, grant number 1DP1AI150593-01 (to H.L.P.).

Author contributions

N. P. and H. L. P. designed and conceived the study. N. P., T. J. H, L. Y. S., W. M., R. J. contributed to data acquisition, analyzed and interpreted the data. L. S. L., A. I, Y. J. X., T. F., N. M., W. P. III, H. R. S contributed to data acquisition. N. P., L. Y. S., R. J., and H. L. P wrote the manuscript with input from all authors.

Competing interests

The authors declare no competing interests.

References

1. Hayter, S.M. and M.C. Cook, *Updated assessment of the prevalence, spectrum and case definition of autoimmune disease.* Autoimmun Rev, 2012. **11**(10): p. 754-65.
2. Morel, L., *Mouse models of human autoimmune diseases: essential tools that require the proper controls.* PLoS Biol, 2004. **2**(8): p. E241.
3. Bonifaz, L.C., et al., *In vivo targeting of antigens to maturing dendritic cells via the DEC-205 receptor improves T cell vaccination.* J Exp Med, 2004. **199**(6): p. 815-24.
4. Idoyaga, J., et al., *Comparable T helper 1 (Th1) and CD8 T-cell immunity by targeting HIV gag p24 to CD8 dendritic cells within antibodies to Langerin, DEC205, and Clec9A.* Proc Natl Acad Sci U S A, 2011. **108**(6): p. 2384-9.
5. Bonifaz, L., et al., *Efficient targeting of protein antigen to the dendritic cell receptor DEC-205 in the steady state leads to antigen presentation on major histocompatibility complex class I products and peripheral CD8+ T cell tolerance.* J Exp Med, 2002. **196**(12): p. 1627-38.
6. Hawiger, D., et al., *Dendritic cells induce peripheral T cell unresponsiveness under steady state conditions in vivo.* J Exp Med, 2001. **194**(6): p. 769-79.
7. Duarte, J.N., et al., *Generation of Immunity against Pathogens via Single-Domain Antibody-Antigen Constructs.* J Immunol, 2016. **197**(12): p. 4838-4847.
8. Van Elssen, C., et al., *Noninvasive Imaging of Human Immune Responses in a Human Xenograft Model of Graft-Versus-Host Disease.* J Nucl Med, 2017. **58**(6): p. 1003-1008.
9. Fang, T., et al., *Structurally Defined alphaMHC-II Nanobody-Drug Conjugates: A Therapeutic and Imaging System for B-Cell Lymphoma.* Angew Chem Int Ed Engl, 2016. **55**(7): p. 2416-20.
10. Ingram, J.R., F.I. Schmidt, and H.L. Ploegh, *Exploiting Nanobodies' Singular Traits.* Annu Rev Immunol, 2018. **36**: p. 695-715.
11. Pishesha, N., J.R. Ingram, and H.L. Ploegh, *Sortase A: A Model for Transpeptidation and Its Biological Applications.* Annu Rev Cell Dev Biol, 2018. **34**: p. 163-188.
12. Villadangos, J.A. and P. Schnorrer, *Intrinsic and cooperative antigen-presenting functions of dendritic-cell subsets in vivo.* Nat Rev Immunol, 2007. **7**(7): p. 543-55.

13. Giralt, M., A. Molinero, and J. Hidalgo, *Active Induction of Experimental Autoimmune Encephalomyelitis (EAE) with MOG35-55 in the Mouse.* Methods Mol Biol, 2018. **1791**: p. 227-232.
14. Boes, M., et al., *T-cell engagement of dendritic cells rapidly rearranges MHC class II transport.* Nature, 2002. **418**(6901): p. 983-8.
15. Moynihan, K.D., et al., *Eradication of large established tumors in mice by combination immunotherapy that engages innate and adaptive immune responses.* Nat Med, 2016. **22**(12): p. 1402-1410.
16. Isaksson, M., et al., *Conditional DC depletion does not affect priming of encephalitogenic Th cells in EAE.* Eur J Immunol, 2012. **42**(10): p. 2555-63.
17. Bodhankar, S., et al., *Estrogen-induced protection against experimental autoimmune encephalomyelitis is abrogated in the absence of B cells.* Eur J Immunol, 2011. **41**(4): p. 1165-75.
18. Hildner, K., et al., *Batf3 deficiency reveals a critical role for CD8alpha+ dendritic cells in cytotoxic T cell immunity.* Science, 2008. **322**(5904): p. 1097-100.
19. Bettelli, E., et al., *Myelin oligodendrocyte glycoprotein-specific T cell receptor transgenic mice develop spontaneous autoimmune optic neuritis.* J Exp Med, 2003. **197**(9): p. 1073-81.
20. Ruffo, E., et al., *Lymphocyte-activation gene 3 (LAG3): The next immune checkpoint receptor.* Semin Immunol, 2019. **42**: p. 101305.
21. Thaker, Y.R., et al., *Treg-specific LAG3 deletion reveals a key role for LAG3 in regulatory T cells to inhibit CNS autoimmunity.* The Journal of Immunology, 2018. **200**(1 Supplement): p. 101.7-101.7.
22. Paterson, A.M., et al., *Deletion of CTLA-4 on regulatory T cells during adulthood leads to resistance to autoimmunity.* J Exp Med, 2015. **212**(10): p. 1603-21.
23. Kim, J.M., J.P. Rasmussen, and A.Y. Rudensky, *Regulatory T cells prevent catastrophic autoimmunity throughout the lifespan of mice.* Nat Immunol, 2007. **8**(2): p. 191-7.
24. Katz, J.D., et al., *Following a diabetogenic T cell from genesis through pathogenesis.* Cell, 1993. **74**(6): p. 1089-100.
25. Maffia, P., et al., *Inducing experimental arthritis and breaking self-tolerance to joint-specific antigens with trackable, ovalbumin-specific T cells.* J Immunol, 2004. **173**(1): p. 151-6.
26. Hogquist, K.A., et al., *T cell receptor antagonist peptides induce positive selection.* Cell, 1994. **76**(1): p. 17-27.
27. Sehrawat, S., et al., *CD8(+) T cells from mice transnuclear for a TCR that recognizes a single H-2K(b)-restricted MHV68 epitope derived from gB-ORF8 help control infection.* Cell Rep, 2012. **1**(5): p. 461-71.
28. Avalos, A.M., et al., *Monovalent engagement of the BCR activates ovalbumin-specific transnuclear B cells.* J Exp Med, 2014. **211**(2): p. 365-79.
29. Bargh, J.D., et al., *Cleavable linkers in antibody-drug conjugates.* Chem Soc Rev, 2019. **48**(16): p. 4361-4374.

30. Florez-Grau, G., et al., *Tolerogenic Dendritic Cells as a Promising Antigen-Specific Therapy in the Treatment of Multiple Sclerosis and Neuromyelitis Optica From Preclinical to Clinical Trials.* Front Immunol, 2018. **9**: p. 1169.
31. Sharrack, B., et al., *Autologous haematopoietic stem cell transplantation and other cellular therapy in multiple sclerosis and immune-mediated neurological diseases: updated guidelines and recommendations from the EBMT Autoimmune Diseases Working Party (ADWP) and the Joint Accreditation Committee of EBMT and ISCT (JACIE).* Bone Marrow Transplant, 2020. **55**(2): p. 283-306.
32. Pishesha, N., et al., *Engineered erythrocytes covalently linked to antigenic peptides can protect against autoimmune disease.* Proc Natl Acad Sci U S A, 2017. **114**(12): p. 3157-3162.
33. Wilson, D.S., et al., *Synthetically glycosylated antigens induce antigen-specific tolerance and prevent the onset of diabetes.* Nat Biomed Eng, 2019. **3**(10): p. 817-829.
34. Kontos, S., et al., *Engineering antigens for in situ erythrocyte binding induces T-cell deletion.* Proc Natl Acad Sci U S A, 2013. **110**(1): p. E60-8.
35. Lorentz, K.M., et al., *Engineered binding to erythrocytes induces immunological tolerance to E. coli asparaginase.* Sci Adv, 2015. **1**(6): p. e1500112.
36. Kishimoto, T.K. and R.A. Maldonado, *Nanoparticles for the Induction of Antigen-Specific Immunological Tolerance.* Front Immunol, 2018. **9**: p. 230.
37. Pearson, R.M., et al., *In vivo reprogramming of immune cells: Technologies for induction of antigen-specific tolerance.* Adv Drug Deliv Rev, 2017. **114**: p. 240-255.
38. Iberg, C.A., A. Jones, and D. Hawiger, *Dendritic Cells As Inducers of Peripheral Tolerance.* Trends Immunol, 2017. **38**(11): p. 793-804.
39. Steinman, R.M., D. Hawiger, and M.C. Nussenzweig, *Tolerogenic dendritic cells.* Annu Rev Immunol, 2003. **21**: p. 685-711.
40. Clemente-Casares, X., et al., *Expanding antigen-specific regulatory networks to treat autoimmunity.* Nature, 2016. **530**(7591): p. 434-40.
41. McCombs, J.R. and S.C. Owen, *Antibody drug conjugates: design and selection of linker, payload and conjugation chemistry.* AAPS J, 2015. **17**(2): p. 339-51.
42. Nicolaou, K.C. and S. Rigol, *The Role of Organic Synthesis in the Emergence and Development of Antibody-Drug Conjugates as Targeted Cancer Therapies.* Angew Chem Int Ed Engl, 2019. **58**(33): p. 11206-11241.
43. Rashidian, M., et al., *Noninvasive imaging of immune responses.* Proc Natl Acad Sci U S A, 2015. **112**(19): p. 6146-51.

Figures

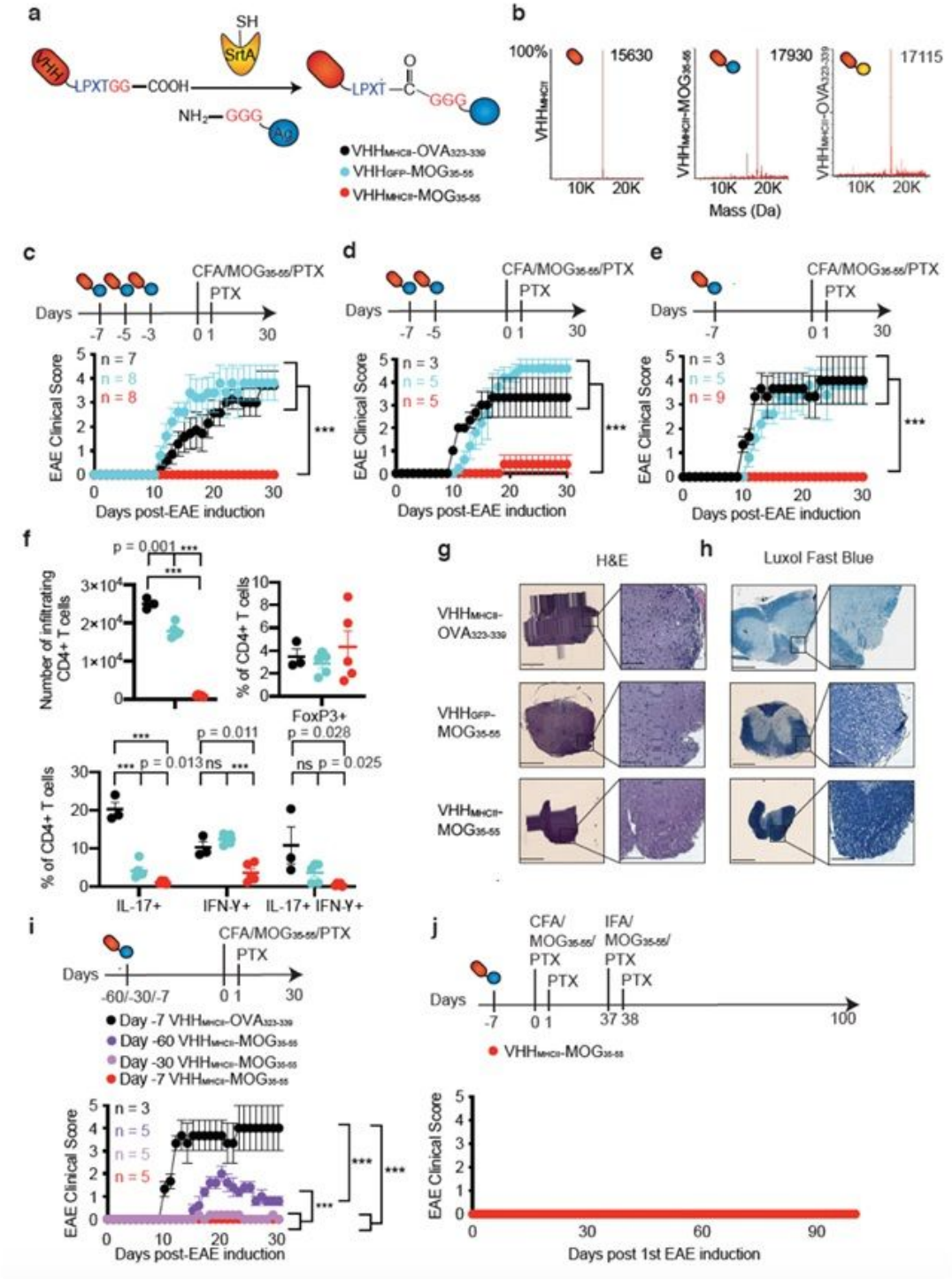

Figure 1

A single dose of VHHMHCII-MOG35-55 provides lasting protection against EAE. a, Schematic for nanobody C-terminal sortase labeling with GGG-carrying antigenic peptides. b, LC-MS of purified VHHMHCII and VHHMHCII-antigen adducts. c, d, e Mean disease scores of mice that received VHH-peptide prophylactic treatment at (c) 3, (d) 2, and (e) 1 dose(s) as indicated. Disease scores: 1, limp tail; 2, partial hind leg paralysis; 3, complete hind leg paralysis; 4, complete hind and partial front leg paralysis;

and 5, moribund. ***, p<0.001, two-way analysis of variance (ANOVA) with repeated measures. f, Flow cytometry of Th1 and Th17 CD4+ lymphocytes in the spinal cord collected at the end point for mice that received 1 dose of VHH-antigen. Frequency of FoxP3+ CD4+ regulatory T cells is also indicated. Data shown as mean ± SEM of biological replicates. n.s. not significant; ***p<0.001, unpaired t test with Holm-Sidak adjustment. g, h, Representative (g) H&E and (h) Luxol Fast Blue staining of spinal cord sections from mice having received a single dose of VHH-antigen adduct. Scale bars, 100mm. i, Mean disease scores of mice that received VHH-peptide prophylactic treatment at -60, -30, and -7 days prior to induction of EAE. j, Mean clinical scores of VHHMHCII-MOG35-55-recipients subjected to multiple challenges with MOG/CFA/PTX and MOG/IFA/PTX. ***p<0.001, two-way analysis of variance (ANOVA) with repeated measures.

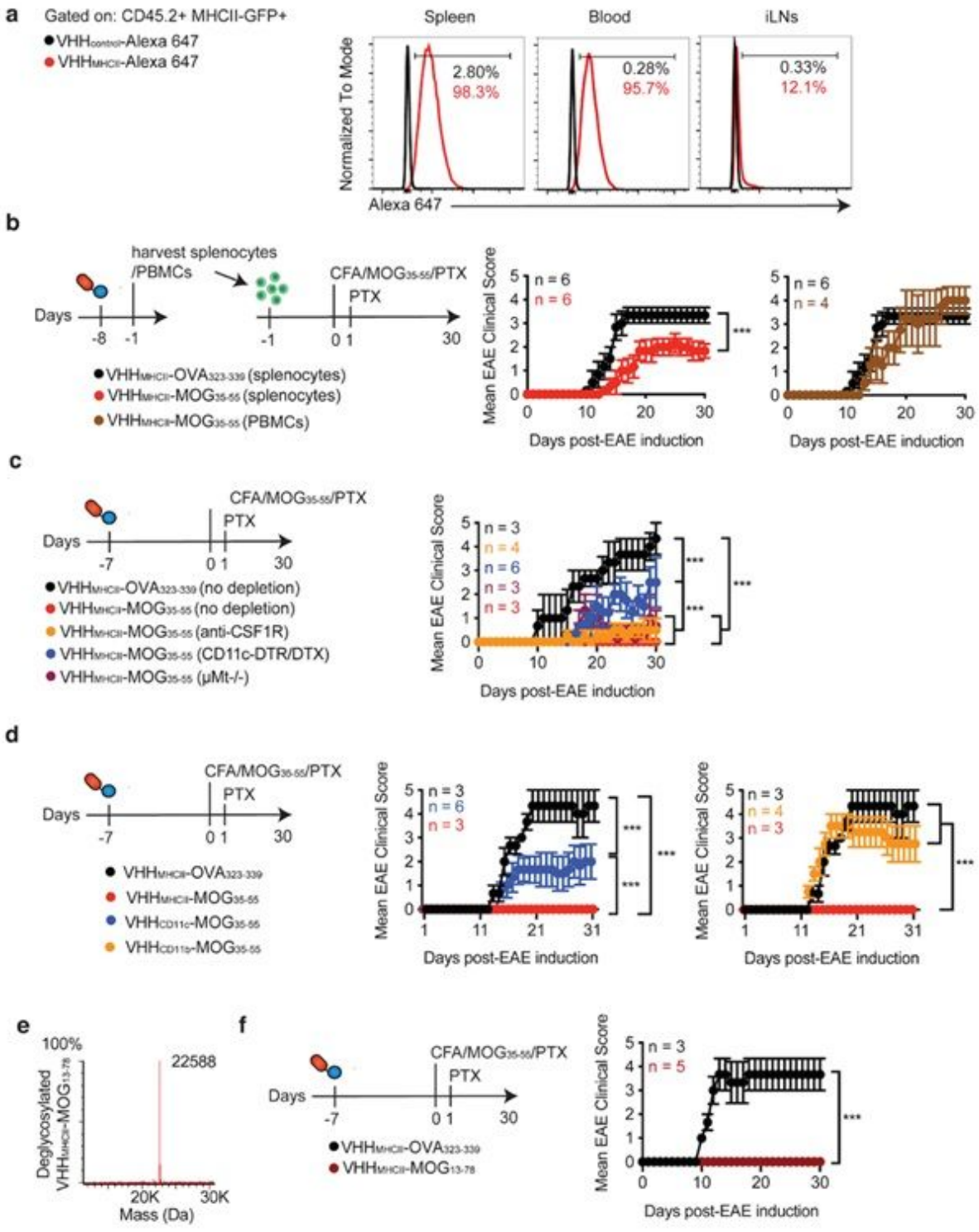

Figure 2

Splenic CD11c+ dendritic cells are responsible for VHHMHCII-MOG35-55 tolerance induction. a, Biodistribution of VHHMHCII in vivo. VHHMHCII-Alexa 647 was injected intravenously into MHCII-GFP mice. 1.5 hours post-injection, spleen, whole blood and inguinal lymph nodes (iLNs) were collected and analyzed by flow cytometry. b, Mean clinical scores of mice that received splenocytes and peripheral blood mononuclear cells (PBMCs) from mice treated with VHHMHCII-OVA323-339 or with VHHMHCII-

MOG35-55. c, Mean clinical scores of mice that received prophylactic treatment with VHHMHCII-OVA323-339 or VHHMHCII-MOG35-55 following depletion of the indicated cell subset prior to induction of EAE. d, Mean disease scores of mice that received the indicated VHH-antigen. e, LC-MS of purified VHHMHCII-MOG17-78. f, Mean disease scores of mice that received VHH-peptide prophylactic treatment. ***p<0.001, two-way analysis of variance (ANOVA) with repeated measures.

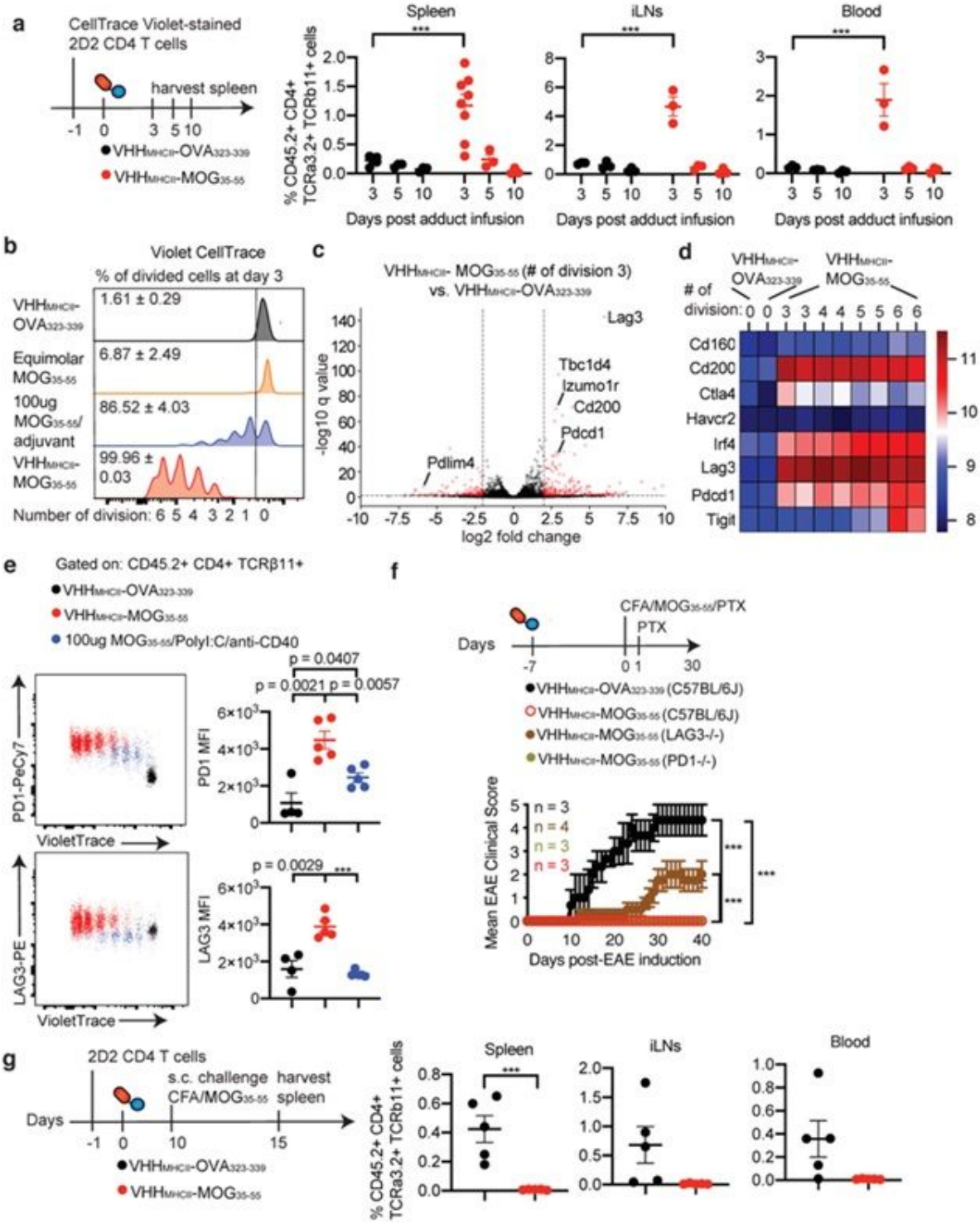

Figure 3

VHHMHCII-MOG35-55 upregulates co-inhibitory receptors on MOG35-55-specific CD4 T cells. a, Congenically marked CD45.1 mice received CellTrace Violet-labeled CD45.2 2D2 CD4 T cells a day prior to infusion of VHH-antigen. We followed the numbers of 2D2 CD4 T cells in spleen, blood, and inguinal lymph nodes (iLNs) by flow cytometry. b, Violet trace dilution indicates proliferation of 2D2 T cells. c, In a separate experiment, on day 3 post infusion, spleens were collected, CD45.2+ CD4+ TCRa3.2+ TCRb11+ cells were sorted according to the number of divisions they underwent and then processed for transcriptomic analyses by RNAseq. Volcano plots of RNA-seq data compare the 2D2 CD4 T cells in mice that received VHHMHCII-MOG35-55 after 3 divisions (div 3) with 2D2 CD4 T cells recovered from mice that received VHHMHCII-OVA323-339. d, Heat map showing the expression of co-inhibitory receptors on 2D2 CD4+ T cells. e, CellTrace Violet-dilution reflects proliferation of 2D2 T cells at day 3. VHHMHCII-MOG35-55 administration leads to a distinct pattern of phenotypic markers on 2D2 CD4 T cells. Representative flow images are shown. The mean fluorescence intensity (MFI) of each marker is plotted as the mean ± SEM of biological replicates. ***p<0.001, unpaired t test with Holm-Sidak adjustment. f, Mean disease scores of mice that received prophylactic treatment with VHHMHCII-OVA323-339 or VHHMHCII-MOG35-55 for the indicated genetic background; ***p<0.001, two-way analysis of variance (ANOVA) with repeated measures. g, We challenged CD45.1 mice that received CD45.2 2D2 CD4 T cells and an infusion of VHH-antigen with MOG35-55 emulsified in CFA on day 10. Spleens, blood, and iLNs were collected 5 days later. 2D2 T cells in mice that had received VHHMHCII-MOG35-55 failed to respond, unlike 2D2 T cells in mice injected with VHHMHCII-OVA323-339. Data are shown as mean ± SEM of biological replicates; ***p<0.001, unpaired t test with Holm-Sidak adjustment.

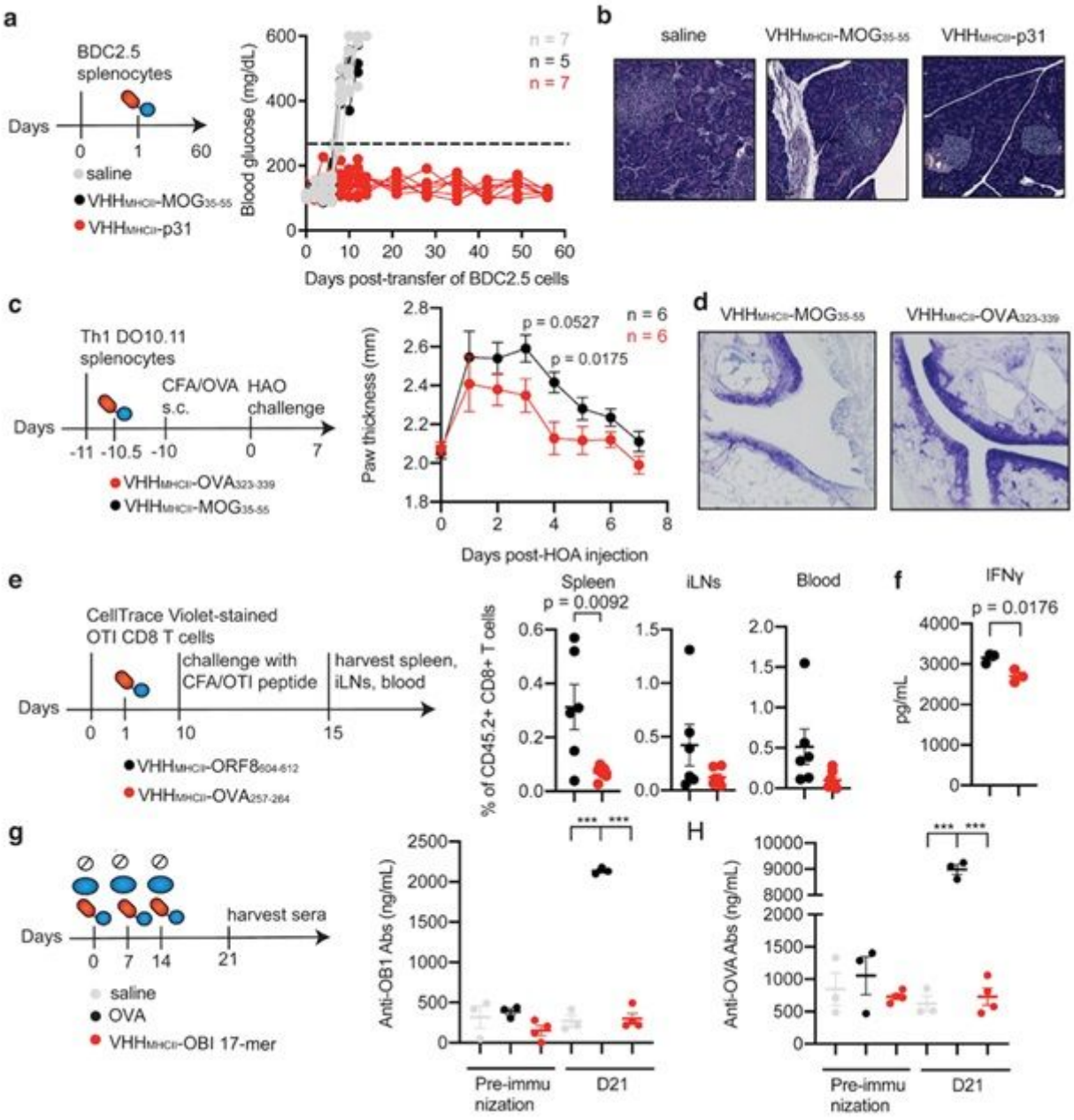

Figure 4

VHHMHCII-antigen-mediated tolerance is antigen specific. a, Blood glucose levels in individual mice treated with VHH-antigen or saline to monitor T1D progression. Mice are considered hyperglycemic when glucose levels are > 260 mg/dL. b, Representative H&E staining of pancreas sections from mice that had received a single dose of VHH-antigen. Scale bars, 100mm. c, Mean paw thickness of Balb/c mice treated with VHH-antigen to assess progression of rheumatoid arthritis. d, Representative Toluidine Blue staining of joint sections from mice that had received a single dose of VHH-antigen. Scale bars, 100mm. e, Mice (CD45.1+) received allotypically marked CD45.2+ CD8+ OTI T cells one day prior to injection of VHHMHCII-ORF8604-612 or VHHMHCII-OVA257-264 (OTI peptide). We challenged these mice with OTI peptide emulsified in CFA on day 10. Spleens, iLNs, and blood were collected 5 days later and analyzed

by flow cytometry. f, Splenocytes were cultured for 3 days in complete RPMI supplemented with OT1 peptide. Supernatant was collected to measure production of IFNg by ELISA. g, h, Antibodies against OB1 peptide (g) and OVA protein (h) were measured by ELISA in sera collected from C57BL/6J recipients that received three consecutive injections of saline, VHHMHCII-OBI, or equimolar amounts of free OVA. Data shown as mean ± SEM of biological replicates. n.s. not significant; ***p<0.001, unpaired t test with Holm-Sidak adjustment.

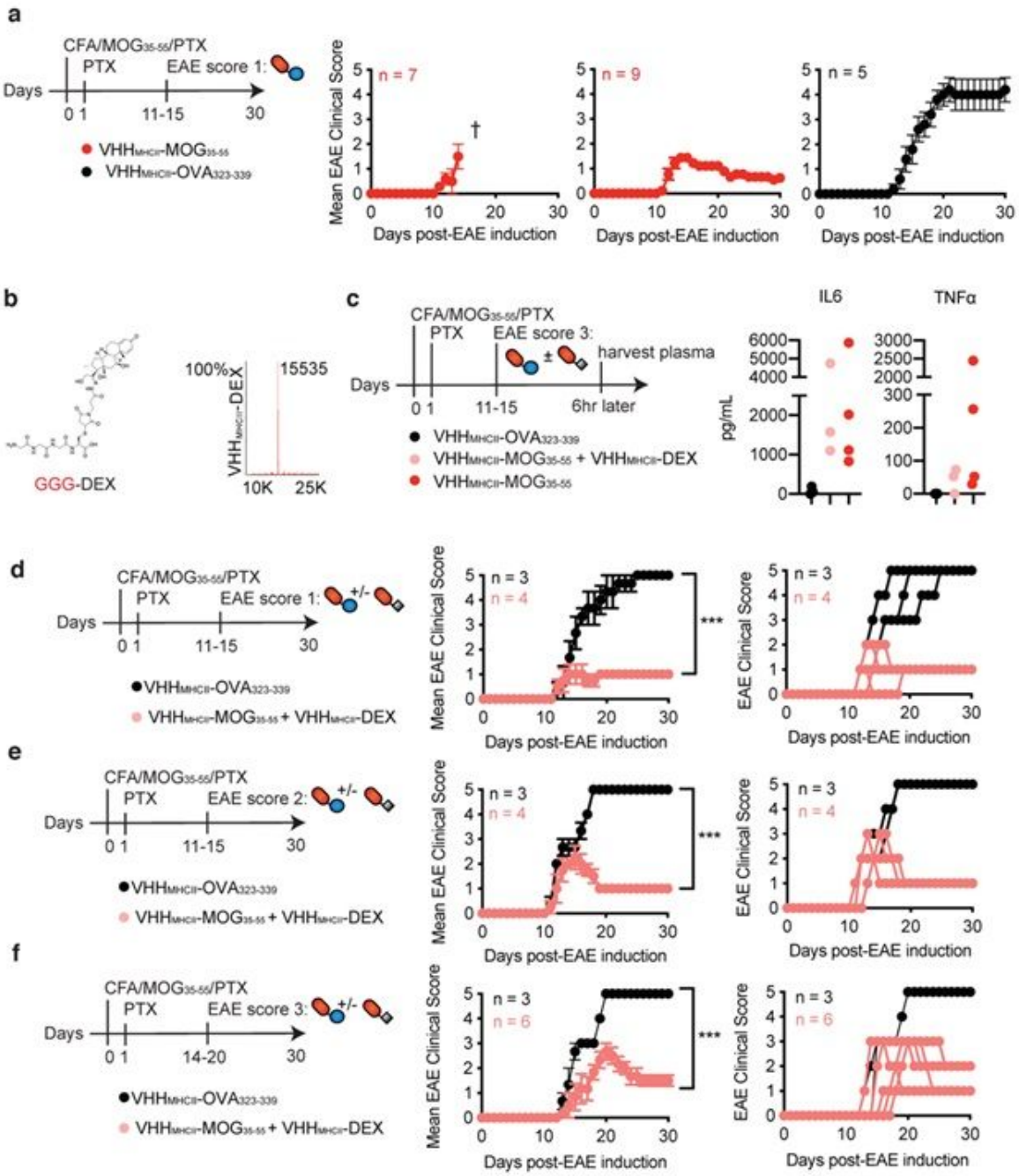

Figure 5

Therapeutic efficacy of VHHMHCII-antigen adducts. a, Mean disease score of mice treated with a single dose of VHHMHCII-MOG35-55 when the animals reached a disease score of 1 (limp tail). ~40% (7/16) of mice succumbed (†), attributed to cytokine storm. b, Structure of GGG-DEX and LC-MS of purified VHHMHCII-DEX. c, Serum levels of TNFa and IL-6 in EAE mice treated with VHH-antigen with or without co-administration of VHHMHCII-DEX. d, e, f, Mean and individual disease score for the mouse cohort treated with a dose of VHH-peptide +/- VHHMHCII-DEX on the day the mouse reached a disease score of (d) 1, (e) 2, or (f) 3. ***, $p<0.001$, two-way analysis of variance (ANOVA) with repeated measures.

Supplementary Files

This is a list of supplementary files associated with this preprint. Click to download.

- ExtendedDataFigures.pdf
- NovaliaPisheshaSupplementaryFigures.pdf